RSC Advances

ROYAL SOCIETY OF CHEMISTRY

www.rsc.org/advances

Journal Name ARTICLE

Synthesis of core-shell ZSM-5@meso-SAPO-34 composite and its application in methanol to aromatics

Cite this: DOI: 10.1039/x0xx00000x

Ling Zhang,[ab] Zhong-Xiang Jiang ,[c] Yue Yu, [c] Chong-Shuai Sun,[c] Yu-Jia Wang,[c] Hai-Yan Wang*[ac]

Received ooth
Accepted ooth

DOI: 10.1039/x0xx00000x

www.rsc.org/

A core/shell-structured ZSM-5@meso-SAPO-34 composite catalyst was hydrothermally synthesized through overgrowing SAPO-34 molecular sieve on the external surface of ZSM-5. The catalyst was thoroughly characterized with regards to their crystallinity, morphology, elemental composition, surface area and pore volume, acidity. The catalytic performance of the as-obtained ZSM-5@meso-SAPO-34 was tested by the conversion of methanol to aromatics reaction. ZSM-5@meso-SAPO-34 exhibited higher aromatics selectivity relative to that of pristine ZSM-5 and its physical mixture with SAPO-34. ZSM-5@meso-SAPO-34's unique catalytic synergistic behaviors were ascribed to having an effective enhancement of aromatization as a result of the acid sites on the external surface covered by SAPO-34 shell.

1. Introduction

Currently, processes like the production of aromatics, including benzene, toluene, and xylene (BTX) are of great significance in the petrochemical industry. Classically, the production of aromatics mainly relies on the catalytic reforming of naphtha. Other alternate processes, such as methanol-to-aromatics (MTA) as replacement for the fossil-based processes have grown to be a new focus for the production of aromatics, owing to the rapid diminishing of fossil resources.[1] Recent studies have demonstrated that methanol can be selectively converted to aromatics by using zeolite-based materials.[2-4]

Aluminosilicate ZSM-5 zeolite, as a shape selective catalyst,[5, 6] has been extensively applied in the fields of petrochemical industry, and the fine chemical industry involving the MTA process. [7] Furthermore, it possesses MFI-type topology connected by two types of 10-membered ring channels, desirable catalytic properties, e.g. high surface area, thermal stability and acidity, as well as adjustable pore size comparable to the molecular dimension of BTX.[8] Accordingly, ZSM-5 zeolite exhibits both higher catalytic activity and remarkable selectivity to aromatics in the process of aromatization.[9-11] However, the catalytic activity and selectivity for aromatics formation are usually alleviated significantly by deactivation and formation of coking associated with carbon deposition, which may lead to the covering of the active sites on the external surface.[12, 13] Additionally, acid sites on the external surface of ZSM-5 can enhance effectively the BTX-selectivity as well as side reactions, which inevitably influence the catalyst BTX-selectivity.[14] Therefore, it is highly desirable to develop suitable catalysts for the production of aromatics. In order to obtain higher catalytic properties, various strategies have been attempted to reduce contributions from external surface acid sites via introduction of mesopores.[15-17] Nevertheless, it may still result in partial destruction and species deposition in the pore structure, consequently influencing zeolite molecular transport properties.

Recent progress has demonstrated that fabrication of core-shell composite materials have paid particular attention to the fields of catalysis due to their acidic properties of the external surface of zeolites and diffusion efficiency can be altered in a desired way.[18-21] Besides, it is noteworthy that core-shell composite materials show their synergetic effects and the multifunctional properties, e.g., nanoarchitectures, alterable compositions and sizes in catalytic reactions. Generally, the synthesis of uniform core-shell materials contains various synthetic approaches such as polytypism and epitaxy or overgrowth.[19, 21-24] Particularly, overgrowth on different materials can combine their different intrinsic properties based on structure and acidity. For instance, ZSM-5/SAPO-11 composites were synthesized by the in situ overgrowth, composed of an acidic H-ZSM-5 zeolite core covered with a SAPO-11 shell.[25] It has been reported previously that the core-shell type composites have desirable acidity, which is favourable to enhance the synergism effect between Brönsted and Lewis acids. In addition, binary structure ZSM-5/SAPO-5 composite zeolites synthesized by overgrowing SAPO-5 over the crystal surface of ZSM-5 have shown a higher propylene yield and conversion of heavy oil, and a striking decrease in the number of surface active sites. [26] More recently, ZSM-5/SAPO-34[27] composites with binary structures have been successfully fabricated employing pre-heated ZSM-5 suspension followed by secondary growth of SAPO-34 layer, which represented excellent catalytic performance and synergetic effect between ZSM-5 and SAPO-34 in propane dehydrogenation reaction.[28] Despite the above described references, reports on the synthesis and application of ZSM-5/SAPO-34 core-shell structure composites are restricted. To the best of our knowledge, the fabrication of this kind of composite zeolites applying overgrowth strategy and its application in the MTA have never been reported before. Silicoaluminophosphate SAPO-34 exhibits higher performance in

methanol-to-olefin (MTO) reactions owing to its characteristic CHA topology and small 8-ring pore (3.8 Å × 3.8 Å) opening, as well as mild acidity.[29, 30] However, the diffusion of bulky molecules such as aromatics in the catalytic reaction severely is hindered by the microporous channels of the SAPO-34 zeolites, probably a result of the presence of the small pores.[31, 32] This limitation could be overcome if the channels of the mesopore SAPO-34 system is introduced in the configuration of the core-shell ZSM-5@SAPO-34.

In this work, we demonstrate a facile two-step hydrothermal synthesis strategy to prepare a series of core–shell heterostructures ZSM-5@meso-SAPO-34 formed by the growth of SAPO-34 crystalline overlayers on ZSM-5 nanocrystals, and mesoporous SAPO-34 layer synthesized using diethylamine (DEA) and tetrapropylammonium hydroxide (TPAOH) as co-templates. The crystallization process of the ZSM-5@meso-SAPO-34 co-crystalline zeolite was systematically investigated via the XRD, SEM, TEM, and nitrogen adsorption characterizations. As a hierarchical-structured composite catalyst, ZSM-5@meso-SAPO-34 exhibits enhanced catalytic properties in the methanol to aromatics with high selectivity for BTX opposed to the mechanical mixing.

2. Experimental

2.1. Material preparation

2.1.1. Synthesis of ZSM-5 and mesoporous SAPO-34.

Zeolite ZSM-5: ZSM-5 crystals with a Si/Al ratio of 25 were synthesized by hydrothermal method. For the typical procedure, colloidal silica sol (30%) was mixed with sodium aluminate and deionized water, and the mixture was stirred for 2 h before tetrapropylammonium hydroxide (TPAOH, >25%) was added. The molar ratio of the reactants in this synthesis was set as $1.0SiO_2$:$0.035Al_2O_3$:$0.07Na_2O$:0.2TPAOH:$30H_2O$. The mixture was vigorously stirred for 4 h before it was transferred into a 100 ml Teflon-line autoclave, which was preheated to 40 °C for 12 h. Zeolite ZSM-5 was then obtained by hydrothermal treatment at 453 K for 48 h under autogenous pressure, after which the products were washed with distilled water and dried at 383 K. The final products were obtained after calcination at 823 K for 5 h to remove any organic substances.

Mesoporous SAPO-34:

Mesoporous SAPO-34 was prepared hydrothermally using DEA and TPAOH as the co-templates with the molar composition of $1.0Al_2O_3$:$1.0P_2O_5$:$0.6SiO_2$:2.0DEA:0.2TEAOH:0.03CTAB:$60H_2O$. TPAOH and DEA was employed as structure directing agent and co-template. Typically, 2.9 g pseudoboehmite (70% Al_2O_3) mixed with the required amount of deionized water was added to 2.7 ml tetraethylorthosilicate (TEOS) under room temperature. After successive stirring for 2 h, 2.7 ml phosphoric acid (85%) was dispersed drop into the above solution with continuous stirring for a further 2 h. subsequently, 3.2 ml TPAOH and 4.2 ml diethylamine (DEA) was added to the mixture, and the mixture was stirred for 5 h. Next, the solution was mixed with an aqueous (80 g of water) solution of CTAB (0.21 g) and stirred for 4 h. Final mixture was transferred into autoclave and aged at 313 K overnight, and then the resulting gel was heated at 453 K for 48 h. All the resulting solid were thoroughly washed with deionized water, filtrated, and dried 12 h at 383 K. The organic template were eliminated by calcination at 823 K for 6 h.

2.1.2. Synthesis of core-shell ZSM-5@meso-SAPO-34. Core-shell ZSM-5@meso-SAPO-34 materials were synthesized by adding amount of premade ZSM-5 precursor into the gel mentioned in SAPO-34 in the absence of TPAOH and DEA. Next, TPAOH and DEA was subsequently added dropwise into the resultant solution under room temperature, then the mixture was dispersed in an aqueous solution of CTAB, continuous stirring until dispersed in a uniformed suspension. After aged at 313 K overnight, the gel was crystallized at 453 K for 1-3 days. Finally, the product was filtrated, washed thoroughly with deionized water, and then dried overnight at 383 K. The organic template were eliminated by calcination at 823 K for 4 h. The final samples were designated CZS (n), where n represents the weight ratio of ZSM-5 precursor and SAPO-34 suspension gel.

2.1.3. Synthesis of mechanical mixture of HZSM-5 and SAPO-34. For control experiment, a mechanical mixture of ZSM-5 and SAPO-34 was prepared by mixing ZSM-5 as-synthesized and amount of mesoporous SAPO-34 as-synthesized with a weight ratio of 2:1.The composite zeolites were calcined at 873 K for 4 h and crushed into 20-40 meshes, and was denoted as HZS.

2.2. Catalyst characterizations

X-ray diffraction (XRD) patterns were performed to determine the phase structures of the samples using D/max –RB diffractometer with Cu-Kα radiation (40 k V, 50 m A). The morphology and size of the crystal materials were measured by scanning electron microscopy (SEM) on a HITACHI SU-8010 microscope equipped with an energy-dispersive X-ray spectrometer (EDS), and operated at 10-15 kV. Transmission electron microscopy (TEM) and high resolution transmission electron microscopy (HRTEM) of the samples were performed on a JEOL JEM-2100F with an acceleration voltage of 200 kV.

Infrared absorption spectra were recorded on a WQF-510 Fourier transform infrared (FT-IR) with the resolution of 4 cm^{-1}. The sample powder and KBr were extruded into the self-supported wafer with the mass ratio of 1:300, and the spectra were recorded in the range of 4000~400 cm^{-1}.N_2 adsorption-desorption isotherms were obtained on a Micromeritics ASAP 2405 analyzer at -196 ℃. Prior to the measurement, each sample (100mg) was degassed at 300℃ for 10 h. The specific surface areas were calculated according to the BET method. The surface area, pore volume of the samples was calculated by BET, t-plot and BJH methods, respectively.

The acidic properties of the samples was determined by NH_3-TPD with a Micromeritics AutoChem II 2920 in the range of 150 ~ 600℃ at a ramp rate of 20 ℃ min^{-1}, and the desorbed ammonia was monitored by a gas chromatograph with a TCD detector.

2.3. Catalytic activity measurement

MTA reaction was carried out in a continuous-flow fixed-bed reactor with inner diameter of 10 mm. The catalyst（5 ml）was loaded into the reactor. Methanol was pumped into the reactor after the catalyst was pretreated in nitrogen flow at 748 k for 3 h. The reaction was conducted under pressure (0.5 MPa), weight hourly space velocity (WHSV =1.2 h^{-1}). Liquid products were analyzed on a gas chromatograph (Agilent 7890A) equipped with a flame ionization detector and a capillary column.

3. Results and discussion

3.1. Preparation and characterization of core-shell ZSM-5@meso-SAPO-34

3.1.1 XRD

ZSM-5@meso-SAPO-34 is prepared with a hydrothermal method by adding an amount of premade ZSM-5 precursor into the gel of SAPO-34. As displayed in Fig.1, the X-ray diffraction patterns of a composite comprising ZSM-5 and SAPO-34 treated for 48 h with the weight ratio of ZSM-5 precursor and SAPO-34 suspension gel varying from 1 to 2. The samples both show well-resolved diffraction peaks at 2θ=7.9°, 8.8°, 22-25°, and 9.5°, which are assigned to the MFI and CHA phases, respectively.[33] The XRD results indicate that the presence of both ZSM-5 and SAPO-34 in the intergrowth zeolites. In addition, it appears that the crystallinity and intensity of CZS-2 are higher than CZS-1. In contrast, the reflections of the ZSM-5@meso-SAPO-34 core-shell are very comparable to those of a mechanical mixture except for weaker relative intensity and crystallinity of the diffraction peak. When compared with those of the pristine zeolites (ZSM-5 and SAPO-34), the characteristic peaks of core-shell ZSM-5@meso-SAPO-34 shift slightly to higher angles due to the distortion of the crystal lattice, in agreement with the XRD analysis the published.[34] In the case of the core-shell zeolite, the shrinkage resulting from intergrowth shows less noticeable due to the ionic radius of silicon is similar to Al and P ions when forming composite zeolites. The observed phenomena evidenced that SAPO-34 has successfully grown as an outer layer of ZSM-5 in CZS simultaneously.

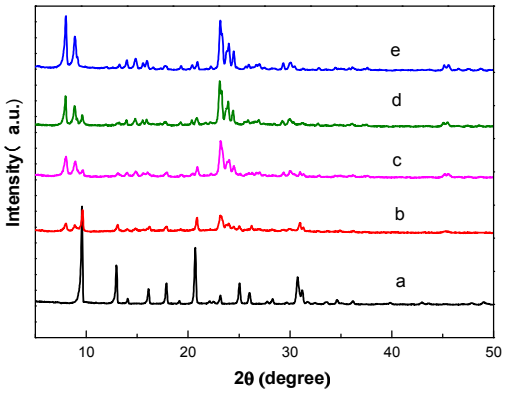

Fig.1. XRD patterns of as-synthesized mesoporous SAPO-34 (a), CZS-1 (b), CZS-2 (c), HZS (d), ZSM-5 (e).

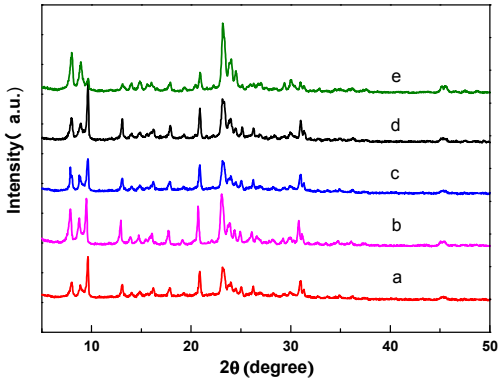

Fig.2. XRD patterns of ZSM-5@meso-SAPO-34 (CZS-2) synthesized at different crystallization time: 24 h (a); 36 h (b); 48 h (c); 60 h (d); 72h (e).

Fig.2 shows XRD patterns of ZSM-5@meso-SAPO-34 (CZS-2) synthesized at different crystallization time, all of which exhibit well-resolved peaks in the range of 5–50°, and match well with those of Fig.1c. With the crystallization time continuously increased, the crystallinity and intensity of CHA in the ZSM-5@meso-SAPO-34 was relatively weaker than that of pure of SAPO-34 crystal, also the intensity of MFI gradually increased. It is observed that the intensity of MFI is higher than that of CHA in Fig-2e. This can be explained as follows: On the one hand, the growth rate of the ZSM-5 phase is fast enough to surpass that of the SAPO-34 phase when crystallization time extended, the former will protrude out of the latter, as shown in Fig. 3e. Therefore, the intensity of MFI is observed higher than CHA. On the other hand, because the weight ratio of ZSM-5 precursor and SAPO-34 suspension gel is 2, which maybe leads to peaks of ZSM-5 are higher than that of SAPO-34 phase during the secondary crystallization process.

3.1.2 SEM and TEM

To further demonstrate the targeted core-shell structure in ZSM-5@meso-SAPO-34, the scanning electron microscope (SEM) was used to characterize the morphology of the as-synthesized. As displayed in Fig.3a, the sample of ZSM-5 as-synthesized possesses very uniform spherical-like morphology with particle sizes ranging from 1 to 2 μm, and consisting of hexagonal columnar monocrystals. Similar morphologies are observed in ZSM-5@meso-SAPO-34 core-shell (Fig.3c-f), and the size of the crystal particle is in agreement with the above. It is attributed to the aggregation of ZSM-5 crystals under the action of Gibbs free energy. In addition, the morphology did not suffer any influence from the gel system of secondary crystallization.

Additionally, Fig.3 mainly displays the morphology of ZSM-5@mesoporous SAPO-34 synthesized during the different crystallization time. Initially, only uniform cubic-like morphology SAPO-34 phase with smooth crystal-face and particle sizes of ca.10μm in diameter was observed in the composite structure after 24 h crystallization (Fig.3b), which is typical morphology of CHA crystalline zeolite. Furthermore, no trace of ZSM-5 crystal was detected on the surface of ZSM-5@ meso-SAPO-34 other than SAPO-34 phase. It was assumed that a layer densely shell of the SAPO-34 formation begins to occur on the surface of ZSM-5 and ZSM-5 further grew into core phase until entirely covered by SAPO-34 shell. However, it did not ensure the core-shell structure only relied on the results. When crystallization time was prolonged to 48 h (Fig.3c-d), spherical ZSM-5 particles began to appear on the surface of ZSM-5@ meso-SAPO-34 and part of particle embedded into the composite structure, which changed the surface of skeletons from smoothness to coarseness. With the crystallization time increased to 72 h (Fig.3e-f), the amount of spherical ZSM-5 particles increased continuously and scattered on the surface of SAPO-34 shell. It suggests that ZSM-5 precursors gradually form in the original silicoaluminophosphate gel of SAPO-34 and further fabricates core-shell composite structure with an increase of crystallization time. Thus, appropriate synthesis time is a critical factor in the synthetic procedure for the forming of self-assembled core-shell structure.

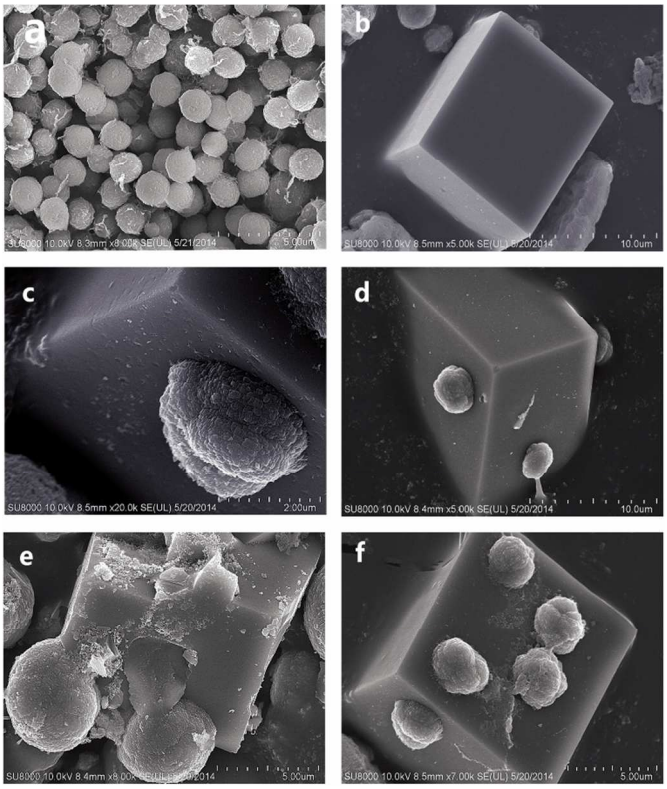

Fig.3. SEM images of ZSM-5 as-synthesized (a), hierarchically mesoporous SAPO-34 (b), core-shell ZSM-5@meso-SAPO-34 (CZS-2) synthesized at different crystallization time: 48 h, high-magnification (c) and corresponding low-magnification (d), 60 h (e), 72 h (f).

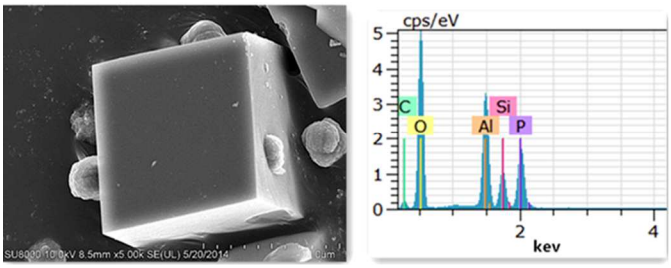

Fig.4. SEM-EDS line scanning of ZSM-5@meso-SAPO-34 core-shell (CZS-2).

The formation of the synthesized core-shell ZSM-5@meso-SAPO-34 was also confirmed by SEM-EDX analysis results presented in Fig.4. Fig.4 reveals that the results of SEM-EDS scanning along the edge of external surface of ZSM-5@meso-SAPO-34 core-shell (CZS-2). According to the data listed in the Fig.4, obviously, a larger number of P element but less Si element were measured on the crystallite surface except for Al element where the P is the chief ingredient of SAPO-34 phase whereas it does not exist in ZSM-5. Thus, the EDS investigation further verified that ZSM-5 phase in the composite may be covered by the SAPO-34 layer generated in the secondary synthesis.

Fig.5 shows the TEM micrographs of the core-shell ZSM-5@ meso-SAPO-34 synthesized, which clearly exhibits the ZSM-5 covered tightly by a about 20-30 nm-thick SAPO-34 shell in a core-shell structure, and no other crystalline phase was detected except the characteristic cubic SAPO-34 phase and few spherical ZSM-5 particles，which in good agreement with SEM results（Fig.3d). Moreover, the lattice fringes between core and shell can be better observed in the enlarged image (Fig.5B). The results indicate that SAPO-34 was grown on the surface of ZSM-5 crystallites successfully and fabricated a core-shell structure composite.

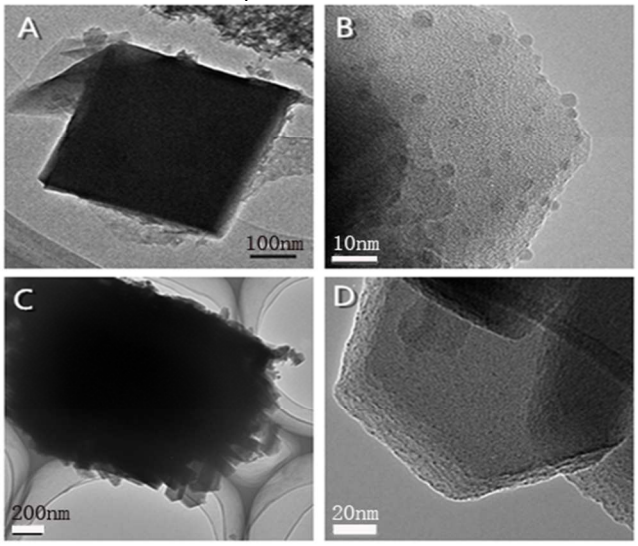

Fig.5. TEM images of core-shell ZSM-5@meso-SAPO-34 (CZS-2) synthesized from crystallization time at 48 h: Low-magnification (A), High-magnification (B), and 72 h Low-magnification (C), High-magnification (D).

3.1.3 FT-IR

FT-IR spectroscopy assists in identifying surface species of shell formed during the crystallization. Fig.6 displays FT-IR spectra of as-synthesized samples of ZSM-5, SAPO-34, ZSM-5@meso-SAPO-34 core-shell (CZS-2) and mechanical mixture (HZS). Framework vibrations at 455, 793 and 1094 cm^{-1} are observed in CZS-2, which corresponds to the Si-O bending mode vibration of tetrahedron inner links of T-O-T similar to those of ZSM-5 zeolites. In addition, two bands at 546 cm^{-1} and 640 cm^{-1} for CZS-2 and HZS are assigned to the asymmetric vibration of the five-membered rings of T–O–T (T=Si or Al) in the MFI frameworks and the bend of double 6-ring, respectively. These results indicate that the core-shell composite sample contains the primary units of CHA zeolites besides MFI-type zeolites, which further proved the forming of shell phase around core phase during the second crystallization.

It's worth noting that distinct absorptions appear at about 1221 cm^{-1}. The peak for CZS-2 slightly shifts to 1218 cm^{-1} and the intensity is lower than those in HZS and pure ZSM-5. This phenomenon can be ascribed to a particular conjunction form of tetrahedrons and a special skeleton structure at the interface between core and shell zeolites. Because the 1221 cm^{-1} IR band is sensitive to change in the zeolite structure, the decrease in intensity proves it maybe includes the presence of CHA structure besides MFI phase. In case of CZS-2 and HZS, all bands exhibit a lower intensity corresponding to pure ZSM-5 and SAPO-34. It is inferred that the introduction of SAPO-34（shell）decreases the crystallinity of synthesized core-shell zeolite, which is in accordance with the result of XRD.

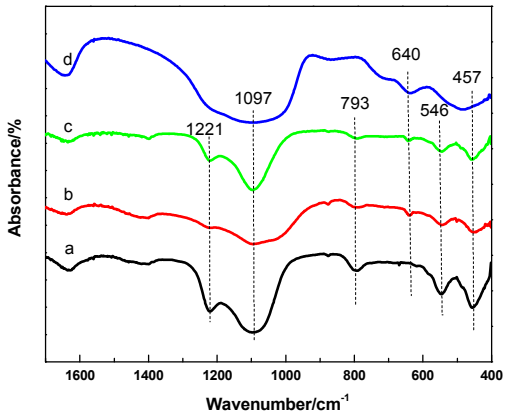

Fig.6. IR spectra of samples: (a) ZSM-5, (b) CZS-2, (c) HZS, (d) mesoporous SAPO-34.

3.1.4 N_2 adsorption-desorption characterization

N_2 adsorption-desorption isotherms and pore size distributions were used to estimate the porosity features of samples shown in Fig.7. The initial part of all samples exhibit the type I isotherm curves with a sharp uptake at relative pressure P/P_0 below 0.1, indicating a characteristic micropore framework. The ZSM-5@meso-SAPO-34 sample displays type IV isotherm with a hysteresis loop at a relative pressure P/P_0 of 0.45-0.95, as a result of the presence of mesopores, which is associated with capillary condensation.[35] Comparatively, the isotherm curves of ZSM-5@meso-SAPO-34 core-shell and mechanical mixture are more or less similar to those of pristine ZSM-5 zeolite combined micropores and mesopores. Whereas, typical hysteresis loops of them obviously show differently. Compared with the latter, the isotherm curve of the core-shell composite sample appears a relatively flat curve with a type H4 hysteresis loop. The phenomenon is associated with narrow slit-like pores in accordance with the IUPAC,[36] which is attributed to the presence of a large number of mesopores in the structured composite. In contrast, the sharp uptake in the adsorption-desorption isotherms of the HZS sample can be observed at higher relative pressure $P/P_0 > 0.9$. Perhaps it arises from the formation of an agglomerate of particles from ZSM-5 and SAPO-34.

The textural properties of samples are listed in Table 1, in which the specific BET surface area and total pore volume of pristine ZSM-5 as-synthesized are 398 m^2g^{-1} and 0.21 cm^3g^{-1} respectively, with lower contribution to mesopores from intrinsic ZSM-5, only 81 $m^2g^{-1}$and 0.13 cm^3g^{-1}, respectively. In contrast, the ZSM-5@meso-SAPO-34 composites possess a lower micropore volumes but more mesopores. The micropore volumes and total pore volumes of ZSM-5@meso-SAPO-34 core-shell are higher than the mechanical mixture, with about 0.16 cm^3g^{-1} and 0.23 cm^3g^{-1}, respectively. It is in accordance with the result of Fig.7.

Table 1 Textual properties of the zeolites samples

Sample	S_{meso}[a] ($m^2.g^{-1}$)	S_{micro}[b] ($m^2.g^{-1}$)	S_{BET}[c] ($m^2.g^{-1}$)	V_{meso}[d] ($cm^3.g^{-1}$)	V_{micro}[e] ($cm^3.g^{-1}$)	V_{total}[f] ($cm^3.g^{-1}$)
ZSM-5	81	317	398	0.08	0.13	0.21
CZS-2	68	309	377	0.16	0.07	0.23
HZS	57	299	356	0.14	0.08	0.22
SAPO-34	52	270	322	0.09	0.16	0.25

[a, b] surface area covered by mesopores and micropores calculated from t-plot, respectively. [c] total surface area calculated using BET equation in a range of relative pressure from 0.05 to 0.3. [d,e] pore volume covered by mesopores and micropores calculated from t-plot; [f] Single point pore volume at P/P_0=0.99.

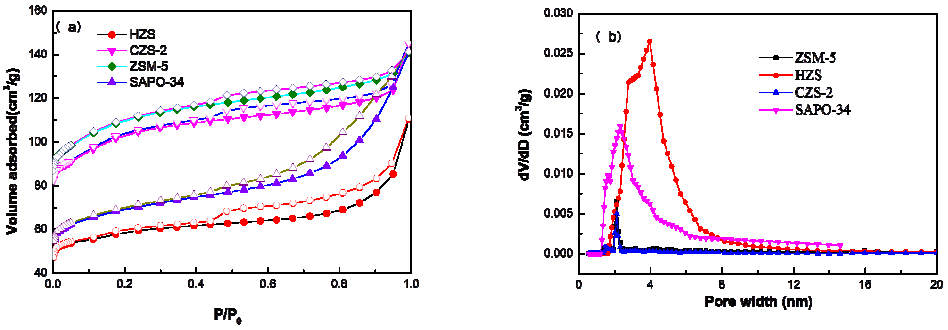

Fig.7. (a) N_2 adsorption-desorption isotherms and (b) pore size distributions of HZS, SAPO-34, CZS-2 and ZSM-5.

Table 2 Product distributions of methanol transformation over the investigated catalysts[a]

Catalyst	Product distribution (wt. %)							Y_{BTX} (%)	S_{BTX} (%)
	C_1-C_5 [b]	B [c]	T [d]	o-X [e]	m-X [f]	p-X [g]	C_9^{+} [h]		
ZSM-5	64.5	2.1	9.8	5.6	9.5	3.1	5.4	30.1	84.7
HZS	62.3	2.9	12.1	6.0	10.8	5.9	5.3	37.7	85.5
SAPO-34	97	0.2	0.2	0.4	1.3	0.4	0.5	2.5	87.1
CZS-1	50.1	3.4	10.5	8.1	14.9	3.3	9.7	40.2	81.5
CZS-1.5	45.8	4.1	11.2	7.9	18.1	4.1	8.8	45.4	83.8
CZS-2	42.9	4.2	13.4	7.9	18.5	4.6	8.5	48.6	85.1
CZS-2.5	43.8	4.3	13.1	7.5	18.2	4.4	8.7	47.5	84.5

[a] Reaction conditions: 0.5 MPa, 460 °C, WHSV=1.2 h^{-1}, time-on-stream = 4 h. [b] C_{1-5} alkenes. [c] Benzene. [d] Toluene. [e] ortho-Xylene. [f] meta-Xylene. [g] para-Xylene. [h] C_9 and C_9^{+} aromatics

3.2 The acidity of ZSM-5@meso-SAPO-34 core–shell catalysts

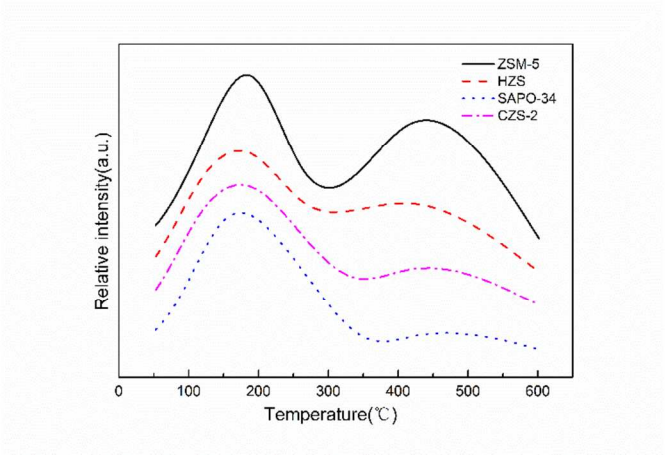

Fig.8. NH_3–TPD patterns of different samples： ZSM-5, CZS-2, HZS and SAPO-34.

The surface acidities of the as-synthesized samples were determined by the temperature programmed desorption of ammonia (NH_3-TPD). As illustrated in Fig.8, the spectrums of the ZSM-5@meso-SAPO-34 display two distinct desorption peaks, the high-temperature peak at ca. 440 ℃ and low-temperature peak centered ca. 183 ℃， which mainly arise from the strong and weak acid sites, respectively. It is can be seen that the area of the high-temperature peak shows an obvious decrease, and simultaneously slightly shifts towards lower temperature relative to that of pristine ZSM-5. It can be deduced that a portion of the strong acid sites of ZSM-5 or the surface of ZSM-5 core may be covered and replaced by the weaker acidity of SAPO-34 shell after the incorporation of SAPO-34, which is in agreement with our previous results. In addition, the mechanical mixture shows lower temperature and smaller acidity relative to that of core-shell ZSM-5@meso-SAPO-34.

3.3 Catalytic performance

Methanol-to-aromatics (MTA) conversion as a typical shape-selective reaction was used to evaluate the catalytic performance of the ZSM-5@mesoporous SAPO-34 catalysts. Its catalytic properties were compared with those of ZSM-5 and physical mixing ZSM-5/SAPO-34 catalysts. As shown in Table 2, SAPO-34 showed an extremely low yield of aromatics (2.5 %) on account of weak acidity as characterized by NH_3-TPD. The yields to aromatics are around 30.1 wt % on parent ZSM-5 zeolites with the Si/Al ratio = 25. However, ZSM-5 exhibits a slightly higher yield of 84.7 wt % to BTX. Compared with the purely acidic ZSM-5, ZSM-5/SAPO-34 (HZS) prepared by physical mixing improves the aromatics yield to 37.7 wt % and gives obviously higher selectivity for BTX (85.5 wt %). In contrast, ZSM-5@meso-SAPO-34 catalyst exhibited high catalytically activity. It is worth noting that the yield to aromatics is obviously enhanced with the increase in ZSM-5/SAPO-34 weight ratio. The selectivity to BTX and yields to aromatics at reaction temperature 460℃ and WHSV=1.2 h^{-1} reach 81.5%, 85.1% and 40.2%, 48.6%, respectively. This result should be related to the increased acidity and acid amount in ZSM-5, which caused the enhancement of aromatics formation. Moreover, the addition of suitable amounts of SAPO-34 in the core-shell structure can be beneficial to aromatics. The direct connection between cores and shells lead to the fabrication of hierarchical porous structure and enhance the accessibility to active sites.

Fig. 9 shows the methanol conversion and selectivity of benzene, toluene, and xylene with time on over ZSM-5@meso-SAPO-34. As presented in the figure, the selectivity of BTX rises with time and can reach the maximum of 85.1% under approaching 100% methanol conversion. Whereas, selectivity levels decrease with time. The change of BTX selectivity could be related to the coking effect, which reduced the pore size of SAPO-34 shell in ZSM-5@meso-SAPO-34.

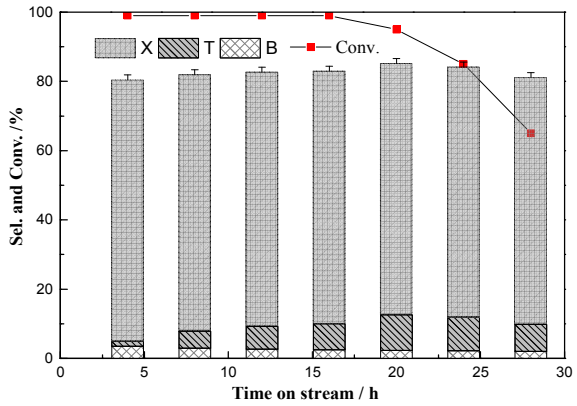

Fig. 9. Conversion and selectivity of BTX with time on stream over ZSM-5@meso-SAPO-34. B: benzene, T: toluene, X: xylene.

4. Conclusions

The hierarchical pore system with core-shell structured ZSM-5@meso-SAPO-34 is successfully prepared by the hydrothermal method via introducing mesoporous SAPO-34 system. The characterization of SEM, BET, XRD, FTIR, TEM, EDS and NH_3-TPD indicated that the cetyltrimethylammonium bromide (CTAB) and TPAOH aided prepared ZSM-5@mesoporous SAPO-34 core-shell composites had large surface area, and high catalytic activity for the MTA. These excellent physicochemical properties for ZSM-5@mesoporous SAPO-34 come from the synergistic effects of ZSM-5 and mesoporous SAPO-34, which shorten diffusion path length within the composites zeolites. Under optimal conditions, the methanol to aromatics on the ZSM-5@mesoporous SAPO-34 achieved a power conversion efficiency of approximately 100% and higher yield of aromatics, which is comparable with the performance of the ZSM-5 and mixture of ZSM-5 and SAPO-34. These results indicate that the ZSM-5@mesoporous SAPO-34 is a promising composite material and provides a novel way for the production of high-value aromatics.

Acknowledgements

This project was financially supported by scientific and technological department of Liaoning Province (No. 201202126).
We appreciate anonymous reviewers for their helpful suggestions on the quality improvement of our present paper.

[a] College of Chemical Engineering, China University of Petroleum, Qingdao 266555, P. R. China. E-mail: fswhy@126.com; Tel: +86-24-56860958

[b] College of Shun Hua , Liaoning Shihua University, Fushun 113001;

[c] College of Chemistry, Chemical Engineering and Environmental Engineering, Liaoning Shihua University, Fushun 113001.

References

1 C. D. Chang, *Catalysis Reviews*, 1983, 25, 1-118.
2 S. Ilias and A. Bhan, *J. Catal.*, 2012, 290, 186-192.
3 M. Conte, J. A. Lopez-Sanchez, Q. He, D. J. Morgan, Y. Ryabenkova, J. K. Bartley, A. F. Carley, S. H. Taylor, C. J. Kiely and K. Khalid, *Catalysis Science & Technology*, 2012, 2, 105-112.
4 Y. Ni, A. Sun, X. Wu, G. Hai, J. Hu, T. Li and G. Li, *Microporous Mesoporous Mater.*, 2011, 143, 435-442.
5 Q. Wang, S. Xu, J. Chen, Y. Wei, J. Li, D. Fan, Z. Yu, Y. Qi, Y. He, S. Xu, C. Yuan, Y. Zhou, J. Wang, M. Zhang, B. Su and Z. Liu, *RSC Advances*, 2014, 4, 21479-21491.
6 N. Y. Chen and W. E. Garwood, *Catalysis Reviews*, 1986, 28, 185-264.
7 A. W. Chester and E. G. Derouane, Zeolite characterization and catalysis, Springer, 2009.
8 G. T. Kokotailo, S. L. Lawton, D. H. Olson and W. M. Meier, *Nature*, 1978, 272, 437-438.
9 M. O. Adebajo and M. A. Long, *Catal. Commun.*, 2003, 4, 71-76.
10 Y. Bi, Y. Wang, X. Chen, Z. Yu and L. Xu, *Chinese Journal of Catalysis*, 2014, 35, 1740-1751.
11 Y. Inoue, K. Nakashiro and Y. Ono, *Microporous Materials*, 1995, 4, 379-383.
12 B. A. Sexton, A. E. Hughes and D. M. Bibby, *J. Catal.*, 1988, 109, 126-131.
13 M. Choi, K. Na, J. Kim, Y. Sakamoto, O. Terasaki and R. Ryoo, *Nature*, 2009, 461, 246-249.
14 W. O. Haag, R. M. Lago and P. B. Weisz, *Nature*, 1984, 309, 589-591.
15 P. Wu, T. Komatsu and T. Yashima, *Microporous Mesoporous Mater.*, 1998, 22, 343-356.
16 R. Chal, C. Gérardin, M. Bulut and S. van Donk, *ChemCatChem*, 2011, 3, 67-81.
17 D. P. Serrano, J. Aguado and J. M. Escola, *in Catalysis*: Volume 23, The Royal Society of Chemistry, 2011, vol. 23, pp. 253-283.
18 D. Van Vu, M. Miyamoto, N. Nishiyama, Y. Egashira and K. Ueyama, *J. Catal.*, 2006, 243, 389-394.
19 Y. Bouizi, I. Diaz, L. Rouleau and V. P. Valtchev, *Adv. Funct. Mater.*, 2005, 15, 1955-1960.
20 Y. Bouizi, L. Rouleau and V. P. Valtchev, *Chem. Mater.*, 2006, 18, 4959-4966.
21 D. Kong, J. Zheng, X. Yuan, Y. Wang and D. Fang, *Microporous Mesoporous Mater.*, 2009, 119, 91-96.
22 L. J. Lauhon, M. S. Gudiksen, D. Wang and C. M. Lieber, Nature, 2002, 420, 57-61.
23. L. Jia, X. Sun, X. Ye, C. Zou, H. Gu, Y. Huang, G. Niu and D. Zhao, Microporous Mesoporous Mater., 2013, 176, 16-24.
24. Y. Lv, X. Qian, B. Tu and D. Zhao, Catal. Today, 2013, 204, 2-7.
25 Y. Fan, D. Lei, G. Shi and X. Bao, *Catal. Today*, 2006, 114, 388-396.
26 Q. Zhang, C. Li, S. Xu, H. Shan and C. Yang, *J. Porous Mater.*, 2013, 20, 171-176.
27 J. Zheng, G. Wang, M. Pan, D. Guo, Q. Zhao, B. Li and R. Li, *Microporous Mesoporous Mater.*, 2015, 206, 114-120.
28 M. Razavian and S. Fatemi, *Microporous Mesoporous Mater.*, 2015, 201, 176-189.
29 Y. Jin, Q. Sun, G. Qi, C. Yang, J. Xu, F. Chen, X. Meng, F. Deng and F. S. Xiao, *Angew. Chem. Int. Ed.*, 2013, 52, 9172-9175.
30 S. Ilias and A. Bhan, *ACS Catalysis*, 2013, 3, 18-31.
31 A. Marchi and G. Froment, *Applied catalysis*, 1991, 71, 139-152.
32 A. Corma, Chem. Rev., 1997, 97, 2373-2420.
33. R. Szostak, Handbook Of Molecular Sieves: Structures, Springer Science & Business Media, 1992.

34 C. Duan, X. Zhang, R. Zhou, Y. Hua, L. Zhang and J. Chen, *Fuel Process. Technol.*, 2013, 108, 31-40.
35 P. Sadeghpour and M. Haghighi, *Particuology*, 2015, 19, 69-81.
36 D. H. E. K. S. W. Sing, R. A. W. Haul, L. Moscou, R. A. Pierotti, J. Rouquerol, T. Siemieniewska, Pure & Appl. Chem, 1985, 57, 603-619.

